AD-A085 761 SRI INTERNATIONAL MENLO PARK CA F/G 18/3
SOME RAMIFICATIONS OF THE POWER-LAW SPECTRAL INDEX FOR PROPAGAT--ETC(U)
OCT 79 C L RINO DNA001-77-C-0038
UNCLASSIFIED DNA-5078T NL

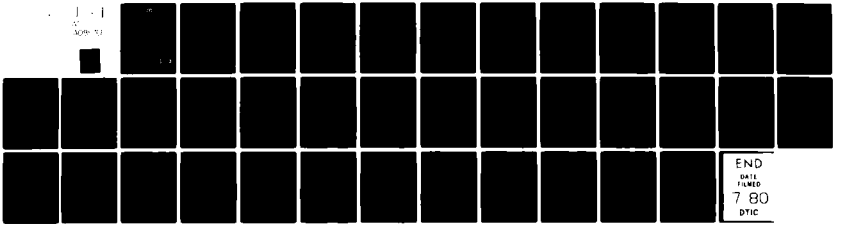

END
DATE FILMED
7 80
DTIC

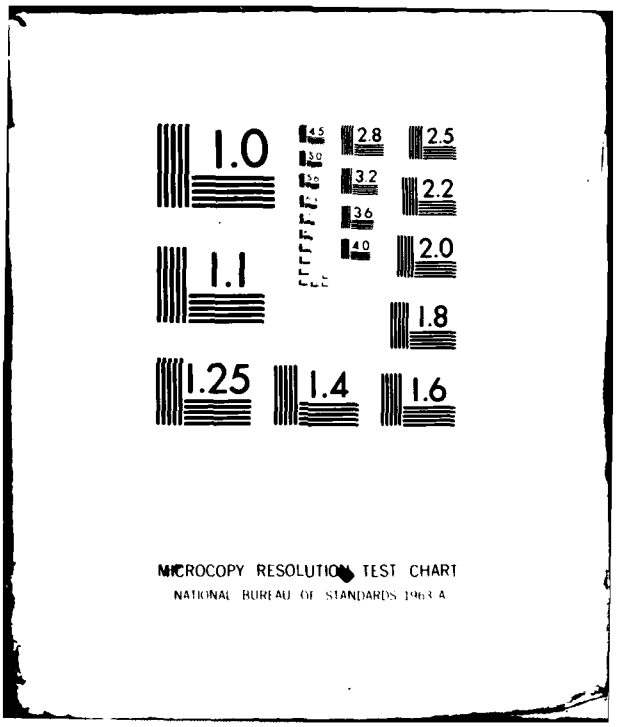
1.0
1.1
1.25
1.4
1.6
1.8
2.0
2.2
2.5
2.8
3.2
3.6
4.0
MICROCOPY RESOLUTION TEST CHART
NATIONAL BUREAU OF STANDARDS 1963 A

(12) LEVEL III

DNA 5078T

SOME RAMIFICATIONS OF THE POWER-LAW SPECTRAL INDEX FOR PROPAGATION MODELING

Charles L. Rino
SRI International
333 Ravenswood Avenue
Menlo Park, California 94025

1 October 1979

Topical Report for Period 1 January 1979— 30 September 1979

CONTRACT No. DNA 001-77-C-0038

APPROVED FOR PUBLIC RELEASE;
DISTRIBUTION UNLIMITED.

THIS WORK SPONSORED BY THE DEFENSE NUCLEAR AGENCY
UNDER RDT&E RMSS CODE B322078464 S99QAXHB05415 H2590D.

Prepared for
Director
DEFENSE NUCLEAR AGENCY
Washington, D. C. 20305

Destroy this report when it is no longer needed. Do not return to sender.

PLEASE NOTIFY THE DEFENSE NUCLEAR AGENCY, ATTN: STTI, WASHINGTON, D.C. 20305, IF YOUR ADDRESS IS INCORRECT, IF YOU WISH TO BE DELETED FROM THE DISTRIBUTION LIST, OR IF THE ADDRESSEE IS NO LONGER EMPLOYED BY YOUR ORGANIZATION.

UNCLASSIFIED

SECURITY CLASSIFICATION OF THIS PAGE (When Data Entered)

REPORT DOCUMENTATION PAGE	READ INSTRUCTIONS BEFORE COMPLETING FORM
1. REPORT NUMBER: DNA 5078T ✓	2. GOVT ACCESSION NO.: AD-A085764
3. RECIPIENT'S CATALOG NUMBER	
4. TITLE (and Subtitle): SOME RAMIFICATIONS OF THE POWER-LAW SPECTRAL INDEX FOR PROPAGATION MODELING	5. TYPE OF REPORT & PERIOD COVERED: Topical Report for Period 1 Jan 79—30 Sep 79
	6. PERFORMING ORG. REPORT NUMBER: SRI Project 5960
7. AUTHOR(s): Charles L. Rino	8. CONTRACT OR GRANT NUMBER(s): DNA 001-77-C-0038 ✓
9. PERFORMING ORGANIZATION NAME AND ADDRESS: SRI International ✓ 333 Ravenswood Avenue Menlo Park, California 94025	10. PROGRAM ELEMENT, PROJECT, TASK AREA & WORK UNIT NUMBERS: Subtask S99QAXHB054-15
11. CONTROLLING OFFICE NAME AND ADDRESS: Director Defense Nuclear Agency Washington, D.C. 20305	12. REPORT DATE: 1 October 1979
	13. NUMBER OF PAGES: 38
14. MONITORING AGENCY NAME & ADDRESS(if different from Controlling Office)	15. SECURITY CLASS (of this report): UNCLASSIFIED
	15a. DECLASSIFICATION DOWNGRADING SCHEDULE

16. DISTRIBUTION STATEMENT (of this Report)

Approved for public release; distribution unlimited.

17. DISTRIBUTION STATEMENT (of the abstract entered in Block 20, if different from Report)

18. SUPPLEMENTARY NOTES

This work sponsored by the Defense Nuclear Agency under RDT&E RMSS Code B322078464 S99QAXHB05415 H2590D.

19. KEY WORDS (Continue on reverse side if necessary and identify by block number)

Scintillation
Power Law

20. ABSTRACT (Continue on reverse side if necessary and identify by block number)

Accurate modeling of radio-wave propagation phenomena is important for verifying our understanding of the physics of ionospheric instabilities that structure the ambient electron density as well as predicting deleterious systems effects. New results in radio-wave propagation theory have quantified the relationship between the power-law index that characterizes the average striation size distribution and the signal structure under strong scatter conditions.

DD FORM 1 JAN 73 1473 EDITION OF 1 NOV 65 IS OBSOLETE

UNCLASSIFIED

SECURITY CLASSIFICATION OF THIS PAGE (When Data Entered)

This report discusses some ramifications for propagation modeling of these new theoretical results. The phase structure function and various functionals of it characterize the striation environment for predictive modeling. Two very different approximations to the phase structure function are currently being used.

One, an asymptotic approximation, is valid when the one-dimensional phase spectral density function falls off less rapidly than f^{-3}. The other, a quadratic approximation derived from the formal Taylor series expansion of the phase structure function, is valid when the one-dimensional phase spectral density function falls off more rapidly than f^{-3}.

The f^{-3} power law marks an important transition in the behavior of the complex signal moments. For the f^{-3} and more steeply sloped phase spectral density functions, the large-scale structure exerts a strong influence on the signal statistics. As a consequence, the outer scale cutoff, which is very difficult to determine, controls the signal parameters that are used to characterize the coherence time, coherence bandwidth, and so forth. This difficulty does not arise for the more shallowly sloped spectral density functions.

Attention is called to the fact that the Wideband satellite data have consistently shown phase spectral density functions that fall off less steeply than f^{-3}, whereas recent barium data from STRESS show more steeply sloped spectra. In light of the impact on propagation modeling, it is important that this discrepancy be resolved. Methods are suggested for testing the consistency of the data analysis procedures used to estimate the phase power-law index.

CONTENTS

ILLUSTRATIONS

I INTRODUCTION

In this report the ramifications of some new theoretical results for modeling late-time, high-altitude nuclear propagation effects are discussed. The results are timely because it appears that there is a systematic difference between (1) the power-law index that characterizes the phase spectrum of radio waves that have propagated through a striated barium environment, and (2) the corresponding power-law index for most radio waves that have propagated through naturally occurring striations in both ionized and nonionized media.

It is generally assumed that the one-dimensional in-situ spectral density function (SDF) that characterizes both naturally occurring and barium striations has the form $\kappa_x^{-2\pm?}$ (Ossakow, 1979)*. For neutral turbulence in the inertial subrange, the Kolmogorov theory predicts $\kappa_x^{-5/3}$, whereas the nonlinear steepening of Rayleigh Taylor and E x B coherent Fourier modes predicts κ_x^{-2}. The number of published in-situ data sets is sparse; however, recently analyzed STRESS data suggest $\kappa_x^{-2.3}$ for barium striation.

If the local in-situ characterization of the irregularities applies throughout the propagation region, then the corresponding one-dimensional integrated-phase SDF has an index one larger than the one-dimensional in-situ index. Thus, the corresponding phase SDF should have the form $f^{-3\pm?}$. The Wideband satellite data have consistently shown comparatively shallow phase SDFs (f^{-p} with $2.2 < p < 2.8$) at all latitudes under highly varied propagation conditions. Similar results are now being reported for interplanetary scintillation and line-of-sight microwave transmissions.

If one accepts the simple mapping from in-situ to phase structure, there is a discrepancy between the in-situ data and the scintillation data. Indeed, the scintillation data suggest an in-situ index smaller

*References are listed at the end of this report.

than the Kolmogorov value. There are good reasons why the simple mapping from in-situ to phase structure might not be invalid, but there is no question that it is the effective slope of the integrated phase SDF that determines the signal structure.

The new theoretical results we have alluded to show that there is a significant change in the signal statistics when the phase spectral slope approaches or exceeds 3. Indeed, the propagation modeling task is potentially much more difficult for steeply sloped spectra. In light of these new developments, it is important that the question of the appropriate effective spectral index for propagation modeling be resolved.

To introduce the problem, consider the common assumption that under conditions of sufficiently strong scatter, the complex signal v(t), is Rayleigh distributed. This means formally that the quadrature components of v(t) are independent, identically distributed, gaussian random processes. Since the second-order statistics completely specify a gaussian random process, one need determine only the mutual coherence function

$$R_v(t,t') = \langle v(t)v^*(t')\rangle \tag{1}$$

to completely characterize the temporal structure of v(t) at a single frequency. In particular, all higher-order signal moments can be computed in terms of $R_v(t,t')$. For example,

$$\langle I(t)I(t')\rangle - \langle I(t)\rangle\langle I(t')\rangle = |R_v(t,t')|^2 \tag{2}$$

where

$$I(t) = |v(t)|^2 \tag{3}$$

is the signal intensity.

It follows from Eq. (2) that the S_4 scintillation index [$S_4^2 = (\langle I^2\rangle - \langle I\rangle^2)/\langle I\rangle^2$] is unity for a Rayleigh process. Thus, if S_4 is not equal to unity, the Rayleigh limit does not apply. Insofar as systems

effects per se are concerned, departures from strict Rayleigh fading are not too serious (Johnson and Rino, 1979). The precise value of the spectral index, however, does impact predictions of time structure, frequency coherence, and so forth. A careful assessment of the signal structure is important, therefore, because it can verify the value that is assigned to the spectral index.

Indeed, Rino (1979b) showed that in a three-dimensional medium with an irregularity spectral density function (SDF) of the form $C_s q^{-(2\nu+1)}$, S_4 converges to unity in the strong-scatter limit if and only if $\nu < 1.5$. When $\nu \geq 1.5$, S_4 achieves a limiting value greater than unity, which can be determined from the formula

$$S_4^2 = \frac{4\sqrt{2\nu - 2}}{5 - 2\nu} \quad . \tag{4}$$

The value $\nu = 1.5$ corresponds to a κ^{-2} one-dimensional in-situ SDF, which, as we have noted, is believed to be associated with steepened irregularity structures. If the $\nu = 1.5$ structure model is assumed to have global applicability, then Eq. (4) predicts the strong-scatter limiting value $S_4 = 1.4$. Since this exceeds unity by 40%, it should be easily detected in any statistically valid data set. Strong focusing, which occurs before the limiting value is achieved, moreover, will cause even larger S_4 values.

In addition to the purely phenomenological impact of the power-law slope, there are ramifications that should effect predictive codes. Indeed, the simple form that is being used for the phase structure function breaks down when $\nu \geq 1.5$.

What is happening can be described intuitively as follows: As the irregularity SDF steepens (ν increases), the importance of the omnipresent large-scale structures steadily increases. If $\nu < 1.5$, these structures manifest themselves only in the first-order moments (e.g., as trend-like phase variations). If $\nu \geq 1.5$, the second-order moments (e.g., the mutual coherence function) develop trend-like components. Finally, if $\nu \geq 2.5$, even the fourth-order moments develop trend-like variations.

The Wideband satellite data clearly favor ν values less than 1.5 as evidently do interplanetary scintillation data, and data from light and microwave propagation through turbulent atmospheres. To accommodate varying ν values, however, a change in the usual approach to propagation modeling is required. Since the mutual coherence function plays a central role in the current approach to predictive modeling, we have developed the theory in detail in this report. The development shows clearly how inhomogeneities manifest themselves and what their impact on predictive modeling is.

II THE MUTUAL COHERENCE FUNCTION

The differential equation that governs the development of the mutual coherence function is

$$\frac{dR_v(\vec{\rho}_1,\vec{\rho}_2)}{dz} = \frac{i}{2k}\left[\nabla_1^2 - \nabla_2^2\right] R_v(\vec{\rho}_1,\vec{\rho}_2) - \frac{1}{2}D(\rho_1,\rho_2)\, R_v(\vec{\rho}_1,\vec{\rho}_2) \quad . \tag{5}$$

In Eq. (5), $\nabla_i^2 = \partial^2/\partial\rho_{x_i}^2 + \partial^2/\partial\rho_{y_i}^2$, $k = 2\pi/\lambda$, and $D(\rho_1,\rho_2)$ is the incremental value of the phase structure function,

$$D(\vec{\rho}_1,\vec{\rho}_2) = \langle[\delta\phi(\vec{\rho}_1) - \delta\phi(\vec{\rho}_2)]\rangle \quad . \tag{6}$$

As discussed by Rino (1978), all the moment equations derived from the parabolic wave equation by using the so-called Markov approximation contain two sets of terms. One set of terms, which involves the Laplacian ∇_i^2, accounts for diffraction effects that act to generate small-scale structure in $v(\vec{\rho})$, particularly in its amplitude. The remaining terms account for the interaction of the wavefield with the randomly irregular medium.

Equation (5) is written in its isotropic form. The general form is developed in Rino (1978). The three-dimensional structure of the wavefield in an anisotropic medium can be derived by straightforward manipulations of the isotropic results (Rino and Fremouw, 1977; Rino, 1978, 1979a). Similarly, the temporal structure of $v(\vec{\rho})$ is readily derived by using an appropriate velocity factor to convert spatial variations to temporal variations.

As a general rule, whenever the diffraction terms impact the solution, the particular moment will depend on the Fresnel factor $\lambda z/4\pi$. From Eq. (5), however, it is readily seen that if $D(\vec{\rho}_1,\vec{\rho}_2)$ depends on the difference variable $\vec{\Delta\rho} = \vec{\rho}_2 - \vec{\rho}_1$, then $R_v(\vec{\rho}_1,\vec{\rho}_2)$ depends only on $\vec{\Delta\rho}$, and

the diffraction terms cancel. It follows that the behavior of $R_v(\vec{\rho}_1,\vec{\rho}_2)$ depends critically on the spatial homogeneity of the structure function.

In most radio-wave modeling work it is assumed without question that any departures of $D(\vec{\rho}_1,\vec{\rho}_2)$ from strict homogeneity can be ignored. To illustrate that there is good reason to question this assumption, consider the signal mean $\langle v(t)\rangle$. The differential equation for $\langle v(t)\rangle$ is

$$\frac{d\langle v(\vec{\rho})\rangle}{dz} = \frac{-i}{2k}\nabla^2\langle v(\vec{\rho})\rangle - \frac{1}{2}r_e^2\lambda^2\langle \Delta N_e(\vec{\rho})\rangle\langle v(\vec{\rho})\rangle \quad . \tag{7}$$

If $\langle \Delta N_e(\vec{\rho})\rangle$ is strictly independent of $\vec{\rho}$, then $\langle v(\vec{\rho})\rangle$ is constant. In fact, one can easily obtain the solution to Eq. (7)--namely,

$$\langle v(\vec{\rho})\rangle = \exp\left[-\frac{1}{2}\langle \delta\phi^2\rangle\right] \tag{8}$$

where

$$\langle \delta\phi^2\rangle = r_e^2\lambda^2 G\ell \int_0^z \langle \Delta N_e^2\rangle \, d\ell \quad . \tag{9}$$

In Eq. (9) G is a purely geometrical factor and ℓ is the first moment of the phase spectral density function.

Whether or not there is a spatial regime where $\langle \Delta N_e(\vec{\rho})\rangle$ can be considered to be constant can only be determined by careful data analysis. Detrending data establishes an arbitrary partitioning between large- and small-scale structures such that the detrended component exhibits all the properties of a homogeneous process. The absolute values of $\langle \delta\phi^2\rangle$ and $\langle v(\vec{\rho})\rangle$, however, are determined by the detrend cutoff. In fact, analysis of the Wideband satellite data has shown that even with detrended data, $\langle v(\vec{\rho})\rangle$ is not well behaved. The estimates show a higher degree of dispersion than the corresponding S_4 estimates. This suggests that the diffraction term in Eq. (7) cannot be ignored.

Going back to the mutual coherence function, if $D(\vec{\rho}_1,\vec{\rho}_2)$ depends only on $\Delta\vec{\rho}$, then one can also easily obtain the solution to Eq. (5)--namely,

$$R_v(\vec{\Delta\rho}) = \exp\left\{-\frac{1}{2}D_{\delta\phi}(\vec{\Delta\rho})\right\} \tag{10}$$

where

$$D_{\delta\phi}(\vec{\Delta\rho}) = r_e^2\lambda^2\int_0^z D(\vec{\Delta\rho})\, d\ell \quad . \tag{11}$$

We note that the initial condition $R_v = 1$ at $z = 0$ is implied by Eq. (10). This effectively normalizes the average signal intensity to unity.

From our experience with the first-order moments $\langle\delta\phi^2\rangle$ and $\langle v\rangle$, we take it as a guiding principle that whenever a computed signal moment of any order depends strongly on q_o, estimators of that quantity will be dependent on how they are measured. The effects are not simply due to uncertainties in the actual value of q_o, but rather to diffraction effects and/or inhomogeneities that can cause significant departures from the mathematical limiting form of the particular moment.

To pursue this further, in Section III we discuss the mathematical model that is being used for the phase structure function.

III THE PHASE STRUCTURE FUNCTION

To simplify the analysis without loss of generality, let us assume that $D(\vec{\rho}_1,\vec{\rho}_2)$ does not vary with z. For a path of length ℓ_p, Eq. (11) then becomes

$$D_{\delta\phi}(\vec{\rho}_1,\vec{\rho}_2) = r_e^2\lambda^2\ell_p \langle[\Delta N_e(\vec{\rho}_1) - \Delta N_e(\vec{\rho}_2)]^2\rangle \quad . \tag{12}$$

The integral can always be reintroduced to accommodate slow variations along the propagation path. The structure function atuomatically enters the theory as discussed in Section II. It has been recognized for some time, however, that the structure function intrinsically suppresss the low-frequency content of the field it is performed on.

To illustrate this directly, consider the one-dimensional form of Eq. (12). It is readily shown that

$$\langle[A(x) - A(x + \Delta x)]^2\rangle = \int [1 - \cos(\omega\Delta x)]\, \Phi_A(\omega)\, \frac{d\omega}{2\pi} \tag{13}$$

where $\Phi_A(\omega)$ is the power spectrum of $A(x)$. Since the cosine term in Eq. (13) varies as ω^2 for small ω, $\Phi_A(\omega) \propto \omega^{-p}$ converges independent of any explicit outer-scale cutoff as long as $p < 3$. This is exactly the behavior of the one-dimensional phase structure functions for which $p = 2\nu$ (Rino, 1979b). It might also be noted that Eq. (13) is identical in form to an MTI (Moving Target Identification) filter that is used for radar clutter suppression.

A convenient SDF model that is both mathematically tractable and accommodates inner-scale and outer-scale cutoffs is

$$\Phi_{\Delta N_e}(q) = C_s q_o^{2\nu+1}\sqrt{1 + (q/q_o)^2}^{(\nu+\frac{1}{2})}\, K_{\nu+\frac{1}{2}}\left(2\epsilon\sqrt{1 + (q/q_o)^2}\right)2\epsilon^{-(\nu+\frac{1}{2})}/\Gamma(\nu+\tfrac{1}{2}) \tag{14}$$

where $\epsilon = q_o/q_i \ll 1$ is the ratio of the inner- to outer-scale cutoffs. By using the small-argument approximation,

$$K_{\nu+\frac{1}{2}}(2x) \sim \frac{1}{2}\,\Gamma(|\nu + \tfrac{1}{2}|)|x|^{-|\nu+\frac{1}{2}|}, \tag{15}$$

it is readily shown that for $q \ll q_i$ and $\epsilon \ll 1$,

$$\Phi_{\Delta N_e}(q) = \frac{C_s}{[q_o^2 + q^2]^{\nu+\frac{1}{2}}} \quad . \tag{16}$$

The phase autocorrelation function corresponding to Eq. (14) is

$$R(y) = \sigma_\phi^2 2\sqrt{\epsilon^2 + (q_o y/2)^2}^{\nu-\frac{1}{2}}\, K_{\nu-\frac{1}{2}}\left(2\sqrt{\epsilon^2 + (q_o y/2)^2}\right)/N \tag{17}$$

where

$$\begin{aligned} N &= 2\epsilon^{\nu-\frac{1}{2}}\, K_{\nu-\frac{1}{2}}(2\epsilon) \\ &\sim \Gamma(\nu - \tfrac{1}{2}) \quad . \end{aligned} \tag{18}$$

The approximation in Eq. (18) is good to within a few percent for $\nu < 0.5$ and $\epsilon < 0.01$. In the small ϵ approximation,

$$\sigma_\phi^2 = r_e^2 \lambda^2 \ell_p C_s \frac{\Gamma(\nu-\frac{1}{2})}{4\pi\Gamma(\nu+\frac{1}{2})}\, q_o^{-2\nu+1} \quad . \tag{19}$$

It is notationally convenient to let

$$C_p = r_e^2 \lambda^2 \ell_p C_s \tag{20}$$

so that the phase SDF has the form $\Phi_{\delta\phi}(q) \sim C_p q^{-(2\nu+1)}$. As noted in Section II, the fact that σ_ϕ^2 depends critically on q_o is indicative of its nonstationary behavior.

The form of the structure function that corresponds to Eq. (17) is

$$\mathcal{D}_{\delta\phi}(y) = 2\sigma_\phi^2 \mathcal{F}(y) = C_p \frac{\Gamma(\nu-\frac{1}{2})}{2\pi\Gamma(\nu+\frac{1}{2})}\left(\frac{\mathcal{F}(y)}{q_o^2 - 1}\right) \tag{21}$$

where

$$\mathcal{F}(y) = 1 - 2\sqrt{\epsilon^2 + (q_o y/2)^2}^{\nu-\frac{1}{2}} K_{\nu-\frac{1}{2}}\left(2\sqrt{\epsilon^2 + (q_o y/2)^2}\right)/N \quad . \tag{22}$$

In Figure 1, $\mathcal{F}(y)$ is plotted versus $q_o y$ for $\nu = 1.2$ and the ϵ values 0.01, 0.001, and 0.0001. It is readily seen that the impact of ϵ is negligible even for comparatively shallow SDFs where its effect is most pronounced. For $\nu = 1.5$, the corresponding curves, which are shown in Figure 2, cannot be distinguished.

Figure 3 shows the effect of varying ν. At first glance the variations are not dramatic. It must be kept in mind, however, that the significant portion of the curve lies to the left of $yq_o = (2\pi)^{-1} = 0.159$, since this corresponds to $y \lesssim \ell_o = 2\pi/q_o$. As ν increases, the curves are displaced to the right of $y = \ell_o$, indicating that structure is being determined more by q_o and less by the power-law slope.

If one accepts the mathematical form of Eq. (22) as being rigorously applicable, the $\mathcal{F}(y)$ curves admit a simple interpretation. Indeed, from Eq. (10), $R_v(\ell_d) = e^{-1}$ when $\sigma_\phi^2 \mathcal{F}(\ell_d) = 1$. It follows that plots of $\mathcal{F}(y)$ versus yq_o are also plots of $1/\sigma_\phi^2$ versus $\ell_d q_o$, provided that $\sigma_\phi > 1$. Since $\mathcal{F}(\ell_d)$ saturates at unity, it is obvious that no meaningful definition of ℓ_d can be obtained for small σ_ϕ values. The fact that the definition of ℓ_d depends on q_o, however, creates problems of its own.

As long as $\nu < 1.5$, there is a simple and effective way to deal with the latter situation that has been used in turbulence studies for over 30 years. It is shown in Appendix B that for sufficiently small q_o,

$$\mathcal{D}_{\delta\phi}(y) \sim C_{\delta\phi}^2 |y|^{2\nu-1} \tag{23}$$

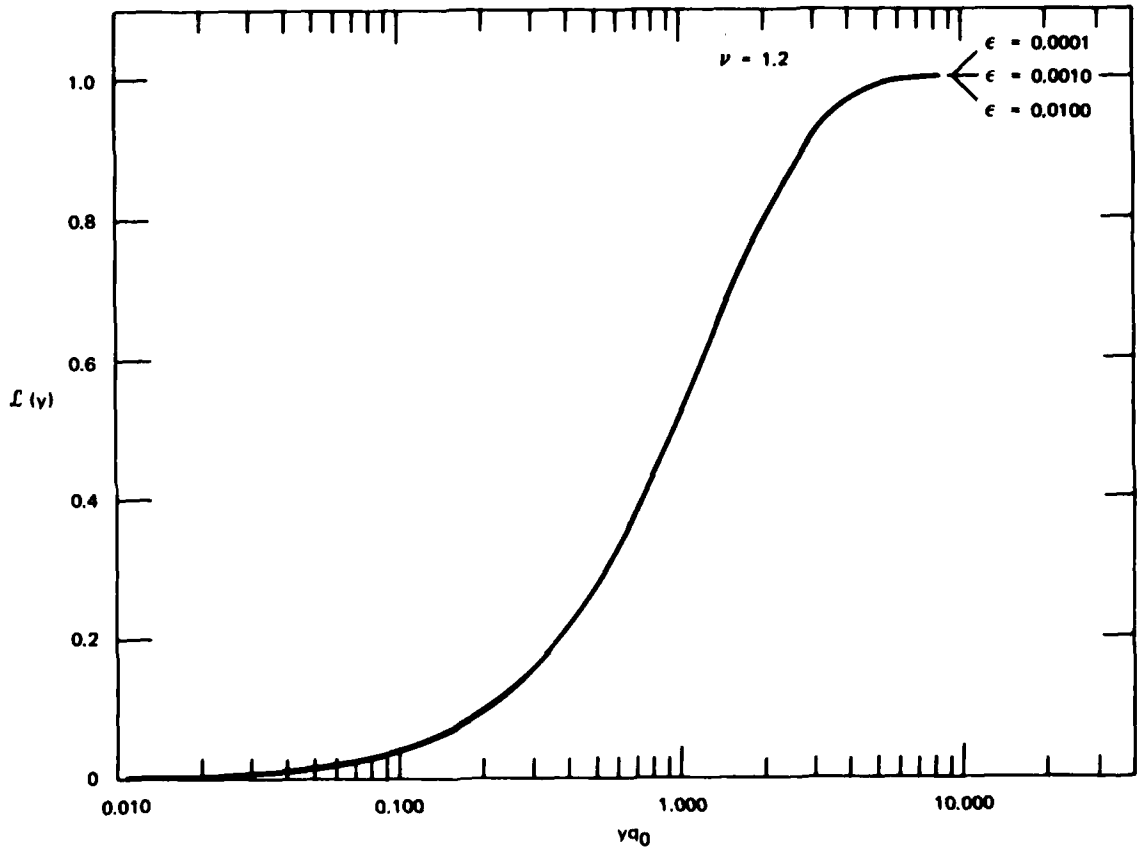

FIGURE 1 PLOT OF NORMALIZED PHASE STRUCTURE FUNCTION SHOWING EFFECT OF ϵ FOR SHALLOWLY SLOPED PHASE SDF

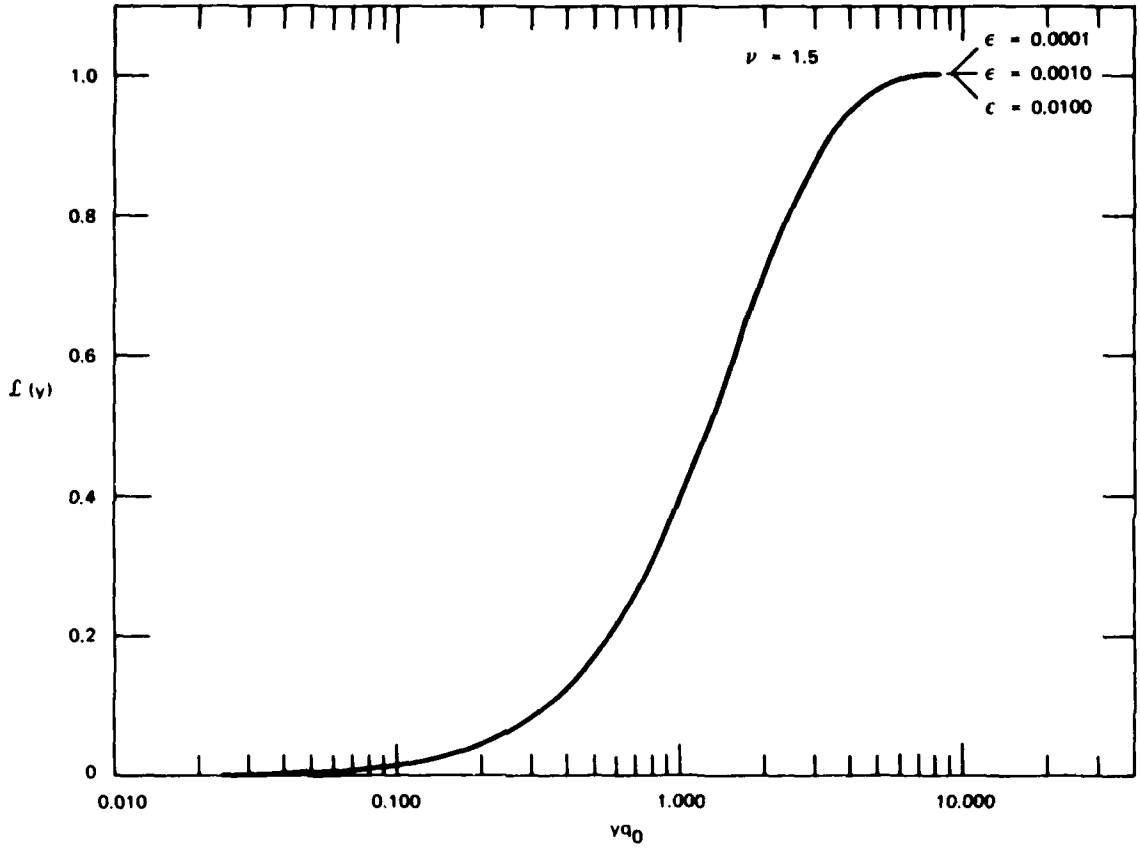

FIGURE 2 PLOT OF NORMALIZED PHASE STRUCTURE FUNCTION SHOWING EFFECT OF ϵ FOR STEEPLY SLOPED PHASE SDF

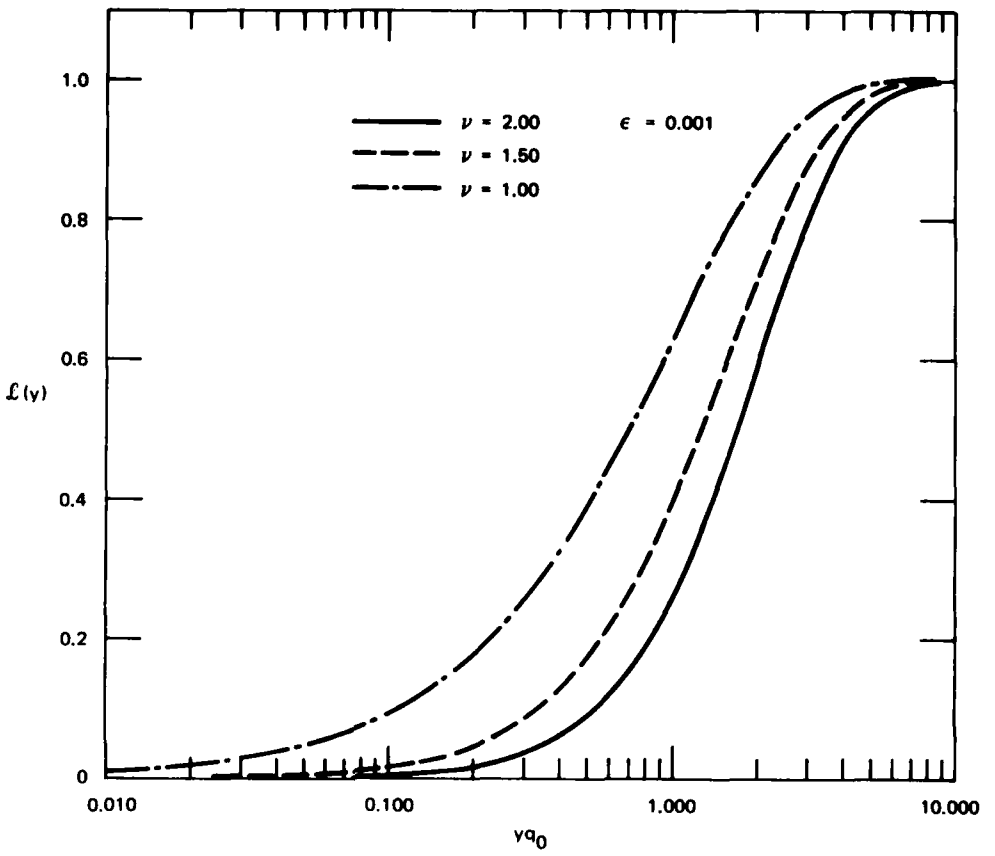

FIGURE 3 PLOT OF NORMALIZED STRUCTURE FUNCTION SHOWING DEPENDENCE ON SPECTRAL SLOPE

where

$$C_{\delta\phi}^2 = \frac{C_p}{2\pi} \frac{2(1.5 - \nu)}{\Gamma(\nu+0.5)(2\nu-1)^{2\nu-1}} \tag{24}$$

is the phase structure constant. To demonstrate the validity of this asymptotic approximation, the approximate form given by Eq. (23) is superimposed on the exact calculation of $\mathcal{L}(y)$ in Figure 4.

The plot is presented on an expanded scale to emphasize the range of y values that contribute to the power-law continuum--viz, $y < \ell$ [$yq_o < 0.159$]. For $\nu \leq 1.2$, the small q_o approximation works essentially over the entire $y \leq \ell_o$ range. As the spectrum steepens ($1.5 > \nu \geq 1.4$), the

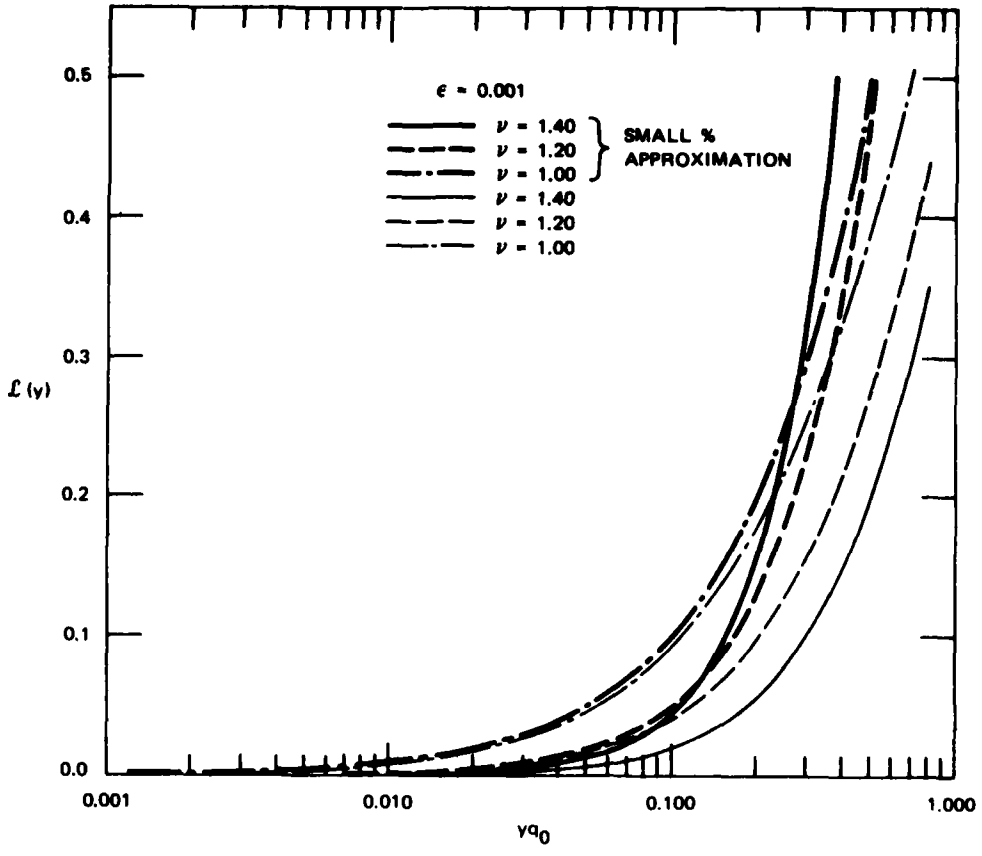

FIGURE 4 PLOT OF SMALL q_0 APPROXIMATION TO PHASE STRUCTION FUNCTION (valid for $\nu < 1.5$) SUPERIMPOSED ON EXACT CURVES

$y \ll \ell_o$ condition becomes more stringent. Thus, as long as $\nu \leq 1.4$, the structure-constant approach is a viable one for the entire range of scale sizes that encompass the power-law continuum.

The ultimate test of any model, however, is how well it reproduces data. The Wideband satellite data have consistently shown p values less than 3. The range of ν for Wideband is $1.2 \leq \nu \leq 1.3$. The Kolmogorov value is $\nu = 4/3 = 1.333$. Excellent results have been obtained in relating the intensity coherence time under strong-scatter conditions to estimates of $C^2_{\delta\phi}$ from the phase data (Rino and Owen, 1979). In the analysis, Eq. (2) was effectively used to relate the intensity structure to $C^2_{\delta\phi}$. Equation (2) was, however, derived by calculating the strong-scatter limiting form of the fourth-order signal moment.

Attempts to measure the mutual coherence function directly have shown that Eq. (10) is strictly valid for a limited range of y values. For example, contrary to the predictions of Eq. (10), measured values of $\langle v(t)v^*(t')\rangle$ invariably go negative. At the present time, attempts are being made to average several estimates together, but it appears that the departures from the idealized model are not simple random fluctuations that ultimately average out to the "correct" value.

What remains is to consider the situation for $\nu \geq 1.5$. As noted in Section I, the radio-wave propagation community has accepted the $\nu = 1.5$ value as a norm, whereas the Wideband satellite data have consistently shown smaller values. The only carefully analyzed data that have indicated steeply sloped SDFs have come from in-situ equatorial rocket probes and in-situ as well as propagation data from the STRESS barium exercises. The early equatorial rocket probes can be dismissed since they only penetrated bottomside spread F. The preliminary results from the recent successful Kwajalein rocket campaign show that bottomside spread-F is a mere ripple when compared with well developed topside structures.

A barium cloud is a highly localized structure whose evolution can be optically tracked. A detailed analysis of the STRESS barium cloud ESTER by MRC has shown, firstly, that structures larger than 1 km cannot be reliably included in the power-law continuum, and secondly, that the smaller-scale structures fall off more steeply than K^{-2}.

The only radio propagation data were obtained from UHF transmissions that were highly disturbed. ESL has used a "back propagation" technique to reconstruct the integrated phase SDF, and the preliminary results seem to be in agreement with the in-situ data in that the phase SDF falls off more steeply than f^{-3}. Under such conditions, however, one should expect significant departures from Rayleigh statistics. The small size of the largest structure may make tests of the statistics difficult. A straightforward test of the back-propagation procedure, however, is to measure the mutual coherence function directly and see how it conforms to model calculations based on $\mathcal{F}(y)$ for $\nu \geq 1.5$.

One would like to believe that the barium data accurately reproduce what it happening locally. Over much larger regions, however, the integration over many structured subregions may well act to produce a shallower integrated phase spectral slope. In that case, the effective ν index for calculating propagation effects is less than 1.5 and the diffraction theory is greatly simplified.

Recent analysis of 30-GHz scintillation data over long atmospheric paths has shown phase spectral slopes significantly lower than the expected 8/3 value based on the Kolmogorov theory. A random patch model has been invoked to reconcile the discrepancy. The model is supported by high-resolution radar data showing that clear-air turbulence develops in distinct narrow regions.

However the issue is resolved, there is a significant discrepancy between structure models inferred from the Wideband satellite data and the structure models that are being extracted from the STRESS barium data. The recent Kwajalein rocket data will undoubtedly shed some light on the issue, but it must be resolved if a viable predictive propagation code is to be developed.

IV THE TAYLOR SERIES APPROXIMATION

Several authors have applied a Taylor series approximation to $\mathcal{L}(y)$ to simplify analyses involving integral expressions containing various combinations of structure functions (e.g., Taylor and Infosino, 1976; Buckley, 1971). As discussed by Rino (1979b), however, these series converge very slowly, particularly in the small q_o limit. In a recent analysis of sound propagation in sea water, Dashen (1977) concluded that the Taylor series approximation cannot be used in power-law medium.

Dashen, however, was concerned with SDF corresponding to $\nu < 1.5$, and the Taylor series approximation improves as ν increases. Indeed, this is expected because the derivatives involved are equivalent to moments in the spectral domain. The moments are increasingly large unless the SDF falls off very rapidly. An inner-scale cutoff keeps the derivatives finite, but the convergence of the series is still very slow if, indeed, proper convergence even occurs.

In any case, the formal Taylor series expansion of $\mathcal{L}(y)$ is easily derived. If we use the notation

$$R_{\nu-\frac{1}{2}}(z) = 2z^{\nu-\frac{1}{2}}K_{\nu-\frac{1}{2}}(2z)/N \tag{25}$$

and

$$f(y) = \sqrt{\epsilon^2 + (yq_o/2)^2} \tag{26}$$

it is shown in Appendix A that

$$\frac{\partial \mathcal{L}(y)}{\partial y} = \mathcal{P}_{\nu-3/2}\left(|f(y)|\right)\ q_o^2 y/2 \quad . \tag{27}$$

From Eq. (27) all higher-order derivatives can be generated. For example,

$$\frac{\partial^2 \mathcal{L}(y)}{\partial y^2} = -\mathcal{R}_{\nu-5/2}(f(y))\ q_o^4 y^2/4 + \mathcal{R}_{\nu-3/2}(f(y))\ q_o^2/2 \quad . \tag{28}$$

In the y = 0 limit, f(y) = ε, and only the even derivatives survive. The formal Taylor series can be written as

$$\mathcal{L}(y) = \sum_{n=1}^{\infty} D_n (q_o y)^{2n} \tag{29}$$

where

$$D_n = \left. \frac{\partial^{2n}\, \mathcal{L}(y)}{(2n)!\partial y^{2n}} \right|_{y\,=\,0} \quad . \tag{30}$$

The coefficients are derived in Appendix A. For our purposes we need consider only the first coefficient,

$$D_1 = \frac{1}{2}\epsilon^{\nu-3/2}\ K_{\nu-3/2}(2\epsilon)/N \tag{31}$$

$$\cong \begin{cases} \dfrac{\Gamma(3/2-\nu)}{4\Gamma(\nu-\frac{1}{2})}\ \epsilon^3 & \nu < 3/2 \\ \dfrac{\log(2\epsilon)}{2\Gamma(\nu-\frac{1}{2})} & \nu = 3/2 \quad . \end{cases} \tag{32}$$

From Eq. (32) we see that for $\nu < 1.5$, D_1 is very sensitive to ε. In fact, the higher-order derivatives are even more sensitive to ε and the Taylor series approach is useless, as noted by Dashen (1977). It appears that the series is divergent except for very small y values. The dependence on ε decreases as ν increases. If $\nu > 1.5$, D_1 does not depend on ε, but higher derivatives do, and convergence problems persist.

In Figure 5 the quadratic approximation is shown for ν = 1.2, 1.5, and 2.0. The approximation is acceptable for ν = 1.5, provided that $y < \ell_o$. It improved as ν exceeds 1.5, but the series approximation cannot be used, as we noted previously. We emphasize that neither the asymptotic nor the quadratic approximation admits y values larger than $\ell_o = 2\pi/q_o$.

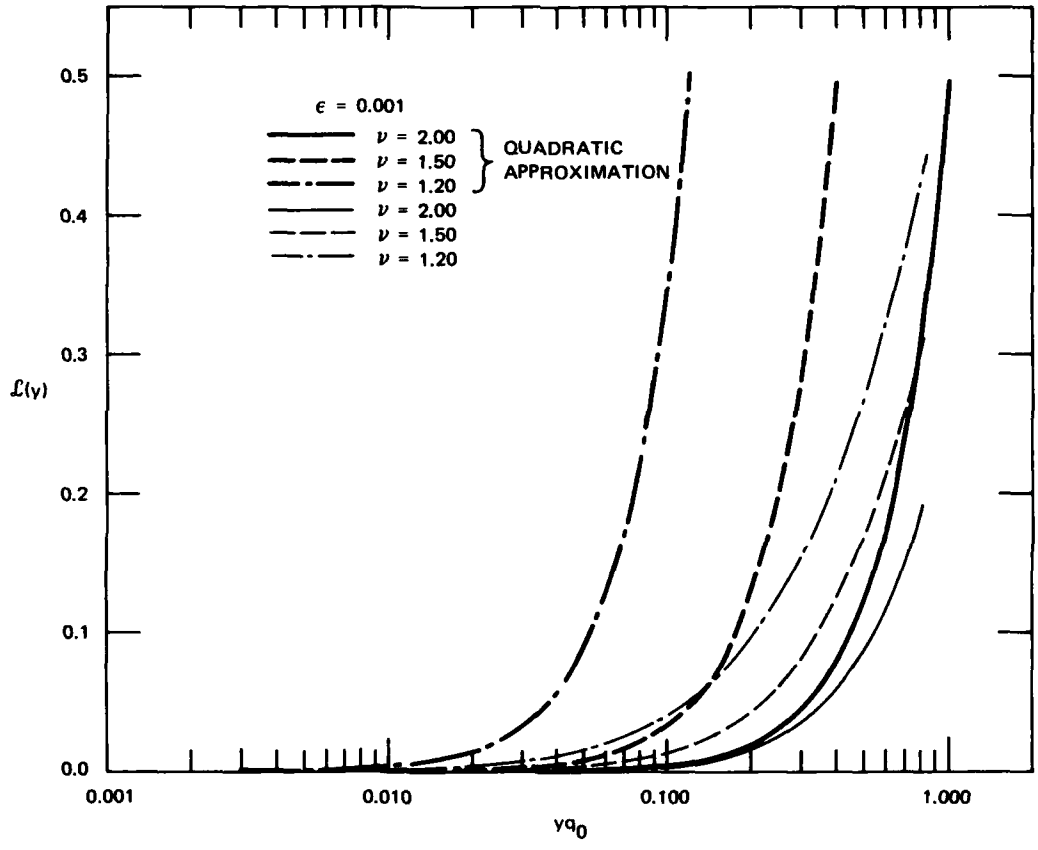

FIGURE 5 PLOT OF QUADRATIC APPROXIMATION TO PHASE STRUCTURE FUNCTION SUPERIMPOSED ON EXACT CURVES

V SUMMARY AND DISCUSSION

In this report we have summarized some new results in propagation theory (Rino, 1979a,b,c; Rino and Owen, 1979), and have discussed their ramifications for predictive modeling. The theory was motivated by the Wideband satellite data which clearly showed the inhomogeneous structure of the integrated electron density. One observes slow trend-like variations in phase because of the dominance of large-scale structures in a power-law environment.

The large-scale structures potentially impact all signal moments. The impact can be nil or totally dominating, depending on the order of the moment and the power-law index. The first-order moment of the complex signal is exponentially dependent on the integrated phase; thus, it exhibits the same nonstationary behavior as the integrated phase.

The second-order complex signal moment (the mutual coherence function), which is used directly or indirectly for predicting essentially all strong-scatter propagation effects, is not sensitive to the large-scale structures if the effective spectral index ν is less than 1.5, which is evidently the case for all naturally occurring irregularities. If $\nu \geq 1.5$ as the STRESS data seem to indicate, the large-scale structures dominate the second-order moments. Predictive modeling then depends critically on the outer-scale parameter.

The Rayleigh hypothesis breaks down when $\nu \geq 1.5$. Insofar as system effects per se are concerned, departures from the gaussian model that is invariably used for analyzing or simulating disturbances are not too important. For predictive modeling of these parameters that characterize the signal structure, however, there is a significant impact.

Because of this fact we have suggested some independent checks of the back-propagation analysis of the STRESS scintillation data. Specifically, the departures from strict Rayleigh statistics, in particular $S_4 > 1$,

that must accompany steeply sloped SDFs should be verified, if possible. The mutual coherence function itself should be carefully measured to verify that it conforms to model predictions.

REFERENCES

Buckley, R., "Diffraction by a Random Phase Screen with Very Large R.M.S. Phase Deviation I. One-Dimensional Screen," Aust. J. Phys., Vol. 24, p. 351, 1971.

Dashen, R., "Path Integrals for Waves in Random Media," Technical Report JSR 76-1, Contract DAHC15-73-C-0370, SRI Project 3000, Stanford Research Institute, Arlington, Va, May 1977.

Johnson, S. C. and C. L. Rino, "Binary Error Rates for a Two-Component Scintillation Channel," Topical Report 3, Contract DNA001-77-C-0038, SRI Project 5960, SRI International, Menlo Park, CA, 1979.

Ossakow, S. L., "Ionospheric Irregularities," Rev. Geophys. Space Phys., Vol. 17, No. 4, p. 521, 1979.

Rino, C. L., "A Power-Law Phase Screen Model for Ionospheric Scintillation 1. Weak Scatter," Radio Science, in press, 1979a.

Rino, C. L., "A Power-Law Phase Screen Model for Ionospheric Scintillation 2. Strong Scatter," Radio Science, in press, 1979b.

Rino, C. L., "Numerical Computations for a One-Dimensional Power-Law Phase Screen," Radio Science, accepted for publication, 1979c.

Rino, C. L., "Iterative Methods for Treating the Multiple Scattering of Radio Waves," J. Atmos. Terr. Phys., Vol. 40, p. 1011, 1978.

Rino, C. L. and E. J. Fremouw, "The Angle Dependence of Singly Scattered Wavefields," J. Atmos. Terr. Phys., Vol. 39, p. 859, 1977.

Rino, C. L. and J. Owen, "The Time Structure of Transionospheric Radiowave Scintillation," submitted to Radio Science, 1979.

Taylor, L. S. and C. J. Infosino, "On the Strong Phase Screen Theory of Ionospheric Scintillations," Radio Science, Vol. 11, No. 5, p. 459, 1976.

Appendix A

THE TAYLOR SERIES APPROXIMATION TO THE PHASE STRUCTURE FUNCTION

The normalized phase structure function can be written as

$$\mathcal{S}(y) = 1 - \mathcal{P}_{\nu-\frac{1}{2}}(f(y)) \tag{A-1}$$

where

$$\mathcal{P}_{\nu-\frac{1}{2}}(z) = 2z^{\nu-\frac{1}{2}} K_{\nu-\frac{1}{2}}(2z)/N \tag{A-2}$$

$$N = 2\epsilon^{\nu-\frac{1}{2}} K_{\nu-\frac{1}{2}}(2\epsilon) \tag{A-3}$$

and

$$f(y) = \sqrt{\epsilon^2 + (q_o y/2)^2} \quad . \tag{A-4}$$

It is clear from Eq. (A-4) that q_o is simply a scale factor. We shall derive a formal Taylor series representation for Eq. (A-1) with the aim of obtaining a simple approximation to $\mathcal{S}(y)$ that is valid for $\epsilon \ll 1$, and as large a yq_o range as possible.

To start with, consider the first derivative,

$$\frac{\partial \mathcal{S}(y)}{\partial y} = - \frac{\partial \mathcal{P}_{\nu-\frac{1}{2}}(f(y))}{\partial y} \quad . \tag{A-5}$$

The derivatives of products such as $z^{\nu-\frac{1}{2}} K_{\nu-\frac{1}{2}}(2z)$ are known, and it is easily shown that

$$\frac{\partial \mathcal{P}\, \alpha\, f(y)}{\partial \mathcal{P}} = -\mathcal{P}_{\alpha-1}(f(y))\, q_o^2 y/2 \quad . \tag{A-6}$$

Using Eq. (A-6) we have

$$\frac{\partial \mathcal{L}(y)}{\partial y} = \mathcal{R}_{\nu-3/2}\,(f(y))\, q_o^2 y/2 \tag{A-7}$$

$$\frac{\partial^2 \mathcal{L}(y)}{\partial y^2} = -\mathcal{R}_{\nu-5/2}\,(f(y))\, q_o^4 y^2/4 + \mathcal{R}_{\nu-3/2}\,(f(y))\, q_o^2/2 \tag{A-8}$$

and

$$\frac{\partial^3 \mathcal{L}(y)}{\partial y^3} = \mathcal{R}_{\nu-7/2}\,(f(y))\, q_o^6 y^3/8 - 2\mathcal{R}_{\nu-5/2}\,(f(y))\, q_o^4 3y/4 \quad . \tag{A-9}$$

The n^{th} derivative of $\mathcal{L}(y)$ has $N_o = (n-1)/2+1$ terms if n is odd, and $N_e = n/2+1$ terms if n is even. The first term always has the form

$$\mathcal{R}_{\nu-1/2-n}\,(f(y))\, q_o^{2n} y^n C_i^n \tag{A-10}$$

where

$$C_i^n = -\,1/2\; C_i^{n-1} \quad . \tag{A-11}$$

We let C_i^n denote the coefficient of the i^{th} term in the n^{th} derivative. If n is odd, the terms i = 2, 3, ..., N_o have the form

$$\mathcal{R}_{(\nu-1/2)-n+(i-1)}\; q_o^{2(n-i+1)}\, y^{(n-2(i-1))}\, C_i^n \tag{A-12}$$

where

$$C_i^n = \left[(n+3-2i)\;\left|C_{q-1}^{n-1}\right| + \frac{1}{2}\left|C_i^{n-1}\right|\right](-1)^{n+2} \quad . \tag{A-13}$$

The same formula, Eq. (A-12), applies to the even derivatives, with the exception that the last coefficient, $C_{n/2+1}^n$, is equal to the previously computed last odd coefficient--i.e.,

$$C^{n}_{n/2+1} = C^{n-1}_{n/2} \quad (n \text{ even}) \quad . \tag{A-14}$$

The formal Taylor series can be written as

$$\mathcal{L}(y) = \sum_{n=1}^{\infty} D_n (yq_o)^{2n} \tag{A-15}$$

where

$$D_n = \left. \frac{\partial^{2n} \mathcal{L}(y)}{(2n)!\ \partial y^{2n}} \right|_{y=0} \quad . \tag{A-16}$$

Only the N_e^{th} even term gives a finite contribution. Hence, from Eq. (A-12)

$$D_n = \frac{1}{(2n)!} \mathcal{R}_{(\nu-1/2)-n}\ f(y)\ |_{y=0}\ C^{2n}_{n+1}$$

$$= \frac{1}{(2n)!}\ \epsilon^{\nu-1/2-n}\ K_{\nu-1/2-n}(2\epsilon)/N\ C^{2n}_{n+1} \quad . \tag{A-17}$$

Note that as long as $\nu-1/2-n > 0$, D_n is nearly independent of ϵ for small ϵ. For large n values, $D_n \propto \epsilon^{2\nu-1-2n}$, which becomes arbitrarily large with increasing n. It follows that the range of applicability of the Taylor series approximation is very restrictive. Recent analysis by Dashen (1977) suggests that it can only be used for propagation environments with a sharp cutoff.

Appendix B

THE SMALL q_o APPROXIMATION

Since $\sigma_\phi \propto q_o^{-2\nu+1}$, it follows that $\sigma_\phi^2(1 - \mathcal{L}(y))$ converges to the indeterminate form $\frac{0}{0}$ when $yq_o << 1$ and q_o is small. If $\nu < 1.5$, however, L'Hopital's rule can be applied to compute the limiting form of $D(y) = \sigma_\phi^2(1 - \mathcal{L}(y))$. We first let $\epsilon \to 0$ to simplify $\mathcal{L}(y)$ to

$$\mathcal{L}(y) \sim 1 - 2|q_o y/2|^{\nu-1/2} K_{\nu-1/2}(q_o y)/\Gamma(\nu-1/2) \qquad \text{(B-1)}$$

which is the form used in Rino (1979b). The quantity of interest is

$$\lim_{q_o \to 0} \frac{\mathcal{L}(y)}{q_o^{2\nu-1}} \quad . \qquad \text{(B-2)}$$

Using the results of Appendix A to calculate the derivative of $\mathcal{L}(y)$, from L'Hopital's rule we have

$$\lim_{q_o \to 0} \frac{\mathcal{L}(y)}{q_o^{2\nu-1}} = \lim_{q_o \to 0} \frac{q_o (q_o y/2)^{\nu-3/2} K_{\nu-3/2}(q_o y) y^2}{\Gamma(\nu-1/2)(2\nu-1) q_o^{2\nu-1}} \quad . \qquad \text{(B-3)}$$

As long as $\nu < 1.5$, the small-argument approximation of $K_{\nu-3/2}(q_o y)$ shows that the q_o terms cancel and we have

$$\lim_{q_o \to 0} \sigma_\phi^2 \delta(y) = \frac{C_p}{2\pi} \frac{2(1.5-\nu)}{\Gamma(\nu+0.5)(2\nu-1)2^{2\nu-1}} |y|^{2\nu-1} \quad . \qquad \text{(B-4)}$$

This result has been used in studies of neutral turbulence for decades. The coefficient that multiplies $|y|^{2\nu-1}$ is the phase structure constant.

In studies involving radio-wave interactions with turbulent neutral atmospheres, only the structure function enters the problem. Indeed, the structure constant is typically modeled directly. Only recently has

serious consideration been given to propagation effects in environments characterized by steeply sloped power-law SDFs.

DISTRIBUTION LIST

DEPARTMENT OF DEFENSE

Assistant Secretary of Defense
Comm., Cmd., Cont. & Intell.
ATTN: C3IST&CCS, M. Epstein
ATTN: Dir. of Intelligence Systems, J. Babcock

Assistant to the Secretary of Defense
Atomic Energy
ATTN: Executive Assistant

Command & Control Technical Center
ATTN: C-312, R. Mason
ATTN: C-650, G. Jones
3 cy ATTN: C-650, W. Heidig

Defense Advanced Rsch. Proj. Agency
ATTN: TIO

Defense Communications Engineer Center
ATTN: Code R720, J. Worthington
ATTN: Code R410, J. McLean
ATTN: Code R123
ATTN: Code R410, R. Craighill

Defense Communications Agency
ATTN: Code 810, J. Barna
ATTN: Code 480
ATTN: Code 101B
ATTN: Code R1033, M. Raffensperger
ATTN: Code 205
ATTN: Code 480, F. Dieter

Defense Technical Information Center
12 cy ATTN: DD

Defense Intelligence Agency
ATTN: DC-7D, W. Wittig
ATTN: DB-4C, E. O'Farrell
ATTN: HO-TR, J. Stewart
ATTN: DB, A. Wise
ATTN: DT-5
ATTN: DT-1B

Defense Nuclear Agency
ATTN: STVL
3 cy ATTN: RAAE
4 cy ATTN: TITL

Field Command
Defense Nuclear Agency
ATTN: FCPR

Field Command
Defense Nuclear Agency
Livermore Division
ATTN: FCPRL

Interservice Nuclear Weapons School
ATTN: TTV

Joint Chiefs of Staff
ATTN: C3S, Evaluation Office
ATTN: C3S

DEPARTMENT OF DEFENSE (Continued)

Joint Strat. Tgt. Planning Staff
ATTN: JLTW-2
ATTN: JSTPS/JLA, R. Haag

National Security Agency
ATTN: R-52, J. Skillman
ATTN: B-3, F. Leonard
ATTN: W-32, O. Bartlett

Undersecretary of Defense for Rsch. & Engrg.
ATTN: Strategic & Space Systems (OS)

WWMCCS System Engineering Org.
ATTN: J. Hoff

DEPARTMENT OF THE ARMY

Assistant Chief of Staff for Automation & Comm.
Department of the Army
ATTN: DAAC-ZT, P. Kenny

Atmospheric Sciences Laboratory
U.S. Army Electronics R&D Command
ATTN: DELAS-EO, F. Niles

BMD Systems Command
Department of the Army
2 cy ATTN: BMDSC-HW

Deputy Chief of Staff for Ops. & Plans
Department of the Army
ATTN: DAMO-RQC

Electronics Tech. & Devices Lab.
U.S. Army Electronics R&D Command
ATTN: DELET-ER, H. Bomke

Harry Diamond Laboratories
Department of the Army
ATTN: DELHD-N-P
ATTN: DELHD-N-RB, R. Williams
ATTN: DELHD-N-P, F. Wimenitz
ATTN: DELHD-I-TL, M. Weiner

U. S. Army Comm.-Elec. Engrg. Instal. Agency
ATTN: CCC-EMEO, W. Nair
ATTN: CCC-EMEO-PED, G. Lane
ATTN: CCC-CED-CCO, W. Neuendorf

U.S. Army Communications Command
ATTN: CC-OPS-W
ATTN: CC-OPS-WR, H. Wilson

U.S. Army Communications R&D Command
ATTN: DRDCO-COM-RY, W. Kesselman

U.S. Army Foreign Science & Tech. Center
ATTN: DRXST-SD

U.S. Army Materiel Dev. & Readiness Command
ATTN: DRCLDC, J. Bender

U.S. Army Nuclear & Chemical Agency
ATTN: Library

DEPARTMENT OF THE ARMY (Continued)

U.S. Army Satellite Comm. Agency
ATTN: Document Control

U.S. Army TRADOC Systems Analysis Activity
ATTN: ATAA-PL
ATTN: ATAA-TCC, F. Payan, Jr.
ATTN: ATAA-TDC

DEPARTMENT OF THE NAVY

Joint Cruise Missile Project Office
Department of the Navy
ATTN: JCM-G-70

Naval Air Development Center
ATTN: Code 6091, M. Setz

Naval Air Systems Command
ATTN: PMA 271

Naval Electronic Systems Command
ATTN: Code 3101, T. Hughes
ATTN: PME 117-20
ATTN: Code 501A
ATTN: PME 117-2013, G. Burnhart
ATTN: PME 117-211, B. Kruger
ATTN: PME 106-4, S. Kearney
ATTN: PME 106-13, T. Griffin

Naval Intelligence Support Center
ATTN: NISC-50

Naval Ocean Systems Center
ATTN: Code 5322, M. Paulson
ATTN: Code 532, J. Bickel
3 cy ATTN: Code 5324, W. Moler

Naval Research Laboratory
ATTN: Code 6700, T. Coffey
ATTN: Code 7550, J. Davis
ATTN: Code 7500, B. Wald
ATTN: Code 6780, S. Ossakow

Naval Space Surveillance System
ATTN: J. Burton

Naval Surface Weapons Center
ATTN: Code F31

Naval Surface Weapons Center
ATTN: Code F-14, R. Butler

Naval Telecommunications Command
ATTN: Code 341

Office of Naval Research
ATTN: Code 420
ATTN: Code 421

Office of the Chief of Naval Operations
ATTN: OP 604C
ATTN: OP 941D
ATTN: OP 981N

Strategic Systems Project Office
Department of the Navy
ATTN: NSP-2722, F. Wimberly
ATTN: NSP-2141
ATTN: NSP-43

DEPARTMENT OF THE AIR FORCE

Aerospace Defense Command
Department of the Air Force
ATTN: DC, T. Long

Air Force Avionics Laboratory
ATTN: AAD, W. Hunt
ATTN: AAD, A. Johnson

Air Force Geophysics Laboratory
ATTN: LKB, K. Champion
ATTN: OPR-1, J. Ulwick
ATTN: PHP, J. Aarons
ATTN: PHI, J. Buchau
ATTN: PHP, J. Mullen
ATTN: OPR, A. Stair

Air Force Weapons Laboratory
Air Force Systems Command
ATTN: DYC
ATTN: SUL

Air Logistics Command
Department of the Air Force
ATTN: OO-ALC/MM, R. Blackburn

Assistant Chief of Staff
Intelligence
Department of the Air Force
ATTN: INED

Assistant Chief of Staff
Studies & Analyses
Department of the Air Force
ATTN: AF/SASC, W. Adams
ATTN: AF/SASC, G. Zank

Deputy Chief of Staff
Operations, Plans & Readiness
Department of the Air Force
ATTN: AFXOXFD
ATTN: AFXOKCD
ATTN: AFXOKT
ATTN: AFXOKS

Deputy Chief of Staff
Research, Development, & Acq.
Department of the Air Force
ATTN: AFRDQ
ATTN: AFRDSP
ATTN: AFRDSS
ATTN: AFRDS

Electronic Systems Division
Department of the Air Force
ATTN: DCKC, J. Clark

Electronic Systems Division
Department of the Air Force
ATTN: XRW, J. Deas

Electronic Systems Division
Department of the Air Force
ATTN: YSM, J. Kobelski
ATTN: YSEA

Foreign Technology Division
Air Force Systems Command
ATTN: TQTD, B. Ballard
ATTN: NIIS, Library
ATTN: SDEC, A. Oakes

DEPARTMENT OF THE AIR FORCE (Continued)

Rome Air Development Center
Air Force Systems Command
ATTN: OCS, V. Coyne
ATTN: TSLD

Rome Air Development Center
Air Force Systems Command
ATTN: EEP

Ballistic Missile Office
Air Force Systems Command
ATTN: MNNL, S. Kennedy
ATTN: MNNH
ATTN: MNNH, M. Baran

Headquarters Space Division
Air Force Systems Command
ATTN: SKA, M. Clavin
ATTN: SKA, C. Rightmyer

Headquarters Space Division
Air Force Systems Command
ATTN: SZJ, L. Doan
ATTN: SZJ, W. Mercer

Strategic Air Command
Department of the Air Force
ATTN: XPFS
ATTN: NRT
ATTN: DCX
ATTN: DCXF
ATTN: DCXT, T. Jorgensen
ATTN: DCXT
ATTN: OOKSN

DEPARTMENT OF ENERGY CONTRACTORS

EG&G, Inc.
ATTN: D. Wright
ATTN: J. Colvin

Lawrence Livermore Laboratory
ATTN: Technical Information Dept.
Library

Los Alamos Scientific Laboratory
ATTN: D. Westervelt
ATTN: P. Keaton
ATTN: R. Taschek

Sandia Laboratories
ATTN: D. Thornbrough
ATTN: D. Dahlgren
ATTN: Org. 1250, W. Brown
ATTN: 3141
ATTN: Space Project Division

Sandia Laboratories
Livermore Laboratory
ATTN: T. Cook
ATTN: B. Murphey

OTHER GOVERNMENT AGENCIES

Central Intelligence Agency
ATTN: OSI/PSTD

Department of Commerce
National Bureau of Standards
ATTN: Sec. Officer for R. Moore

OTHER GOVERNMENT AGENCIES (Continued)

Department of Commerce
National Oceanic & Atmospheric Admin.
ATTN: R. Grubb

Institute for Telecommunications Sciences
National Telecommunications & Info. Admin.
ATTN: L. Berry
ATTN: A. Jean
ATTN: W. Utlaut
ATTN: D. Crombie

U.S. Coast Guard
Department of Transportation
ATTN: G-DOE-3/TP54, B. Romine

DEPARTMENT OF DEFENSE CONTRACTORS

Aerospace Corp.
ATTN: F. Morse
ATTN: N. Stockwell
ATTN: I. Garfunkel
ATTN: D. Olsen
ATTN: S. Bower
ATTN: T. Salmi
ATTN: R. Slaugher
ATTN: V. Josephson

University of Alaska
ATTN: Technical Library
ATTN: T. Davis
ATTN: N. Brown

Analytical Systems Engineering Corp.
ATTN: Radio Sciences

Analytical Systems Engineering Corp.
ATTN: Security

Barry Research Communications
ATTN: J. McLaughlin

BDM Corp.
ATTN: L. Jacobs
ATTN: T. Neighbors

Berkeley Research Associates, Inc.
ATTN: J. Workman

Boeing Co.
ATTN: M/S 42-33, J. Kennedy
ATTN: S. Tashird
ATTN: G. Hall

University of California at San Diego
ATTN: H. Booker

Charles Stark Draper Lab., Inc.
ATTN: D. Cox
ATTN: J. Gilmore

Computer Sciences Corp.
ATTN: H. Blank

Comsat Labs.
ATTN: G. Hyde
ATTN: R. Taur

Cornell University
ATTN: D. Farley, Jr.

DEPARTMENT OF DEFENSE CONTRACTORS (Continued)

Electrospace Systems, Inc.
ATTN: H. Logston

ESL, Inc.
ATTN: C. Prettie
ATTN: J. Roberts
ATTN: J. Marshall

Ford Aerospace & Communications Corp.
ATTN: J. Mattingley

General Electric Co.
ATTN: M. Bortner

General Electric Co.
ATTN: F. Reibert

General Electric Company-TEMPO
ATTN: W. Knapp
ATTN: M. Stanton
ATTN: T. Stevens
ATTN: D. Chandler
ATTN: DASIAC

General Electric Tech. Services Co., Inc.
ATTN: G. Millman

General Electric Co.
ATTN: C. Zierdt
ATTN: A. Steinmayer

General Research Corp.
ATTN: J. Ise, Jr.
ATTN: J. Garbarino

GTE Sylvania, Inc.
ATTN: M. Cross

HSS, Inc.
ATTN: D. Hansen

IBM Corp.
ATTN: F. Ricci

University of Illinois
ATTN: Security Supervisor for K. Yeh

Institute for Defense Analyses
ATTN: E. Bauer
ATTN: [illegible]. Aein
ATTN: [illegible]. Bengston
ATTN: H. Wolfhard

International Tel. & Telegraph Corp.
ATTN: Technical Library
ATTN: G. Wetmore

JAYCOR
ATTN: [illegible]. Goldman

JAYCOR
ATTN: D. Carlos

Johns Hopkins University
ATTN: T. Potemra
ATTN: Document Librarian
ATTN: P. Komiske
ATTN: J. Evans
ATTN: J. Newland
ATTN: P. Wise

DEPARTMENT OF DEFENSE CONTRACTORS (Continued)

Kaman Sciences Corp.
ATTN: T. Meagher

Linkabit Corp.
ATTN: I. Jacobs

Litton Systems, Inc.
ATTN: R. Grasty

Lockheed Missiles & Space Co., Inc.
ATTN: Dept. 60-12
ATTN: D. Churchill

Lockheed Missiles and Space Co., Inc.
ATTN: R. Johnson
ATTN: M. Walt
ATTN: W. Imhof

M.I.T. Lincoln Lab.
ATTN: D. Towle
ATTN: L. Loughlin

McDonnell Douglas Corp.
ATTN: N. Harris
ATTN: G. Mroz
ATTN: J. Moule
ATTN: W. Olson

Meteor Communications Consultants
ATTN: R. Leader

Mission Research Corp.
ATTN: R. Hendrick
ATTN: S. Gutsche
ATTN: F. Fajen
ATTN: D. Sowle
ATTN: R. Bogusch

Mitre Corp.
ATTN: C. Callahan
ATTN: G. Harding
ATTN: A. Kymmel
ATTN: B. Adams

Mitre Corp.
ATTN: W. Foster
ATTN: M. Horrocks
ATTN: W. Hall

Pacific-Sierra Research Corp.
ATTN: E. Field, Jr.

Pennsylvania State University
ATTN: Ionospheric Research Lab.

Photometrics, Inc.
ATTN: I. Kofsky

Physical Dynamics, Inc.
ATTN: E. Fremouw

R & D Associates
ATTN: B. Yoon
ATTN: C. Delaney

Rand Corp.
ATTN: C. Crain
ATTN: E. Bedrozian

DEPARTMENT OF DEFENSE CONTRACTORS (Continued)

R & D Associates
ATTN: R. Lelevier
ATTN: B. Gabbard
ATTN: R. Turco
ATTN: F. Gilmore
ATTN: H. Ory
ATTN: W. Karzas
ATTN: W. Wright, Jr.
ATTN: C. MacDonald
ATTN: C. Greifinger
ATTN: M. Gantsweg

Riverside Research Institute
ATTN: V. Trapani

Rockwell International Corp.
ATTN: J. Kristof

Santa Fe Corp.
ATTN: E. Ortlief

Science Applications, Inc.
ATTN: L. Linson
ATTN: D. Hamlin
ATTN: D. Sachs
ATTN: E. Straker
ATTN: J. McDougall
ATTN: C. Smith

Science Applications, Inc.
ATTN: SZ

Science Applications, Inc.
ATTN: D. Divis

DEPARTMENT OF DEFENSE CONTRACTORS (Continued)

SRI International
ATTN: R. Livingston
ATTN: G. Smith
ATTN: G. Price
ATTN: R. Leadabrand
ATTN: W. Jaye
ATTN: W. Chesnut
ATTN: M. Baron
ATTN: A. Burns
ATTN: D. Neilson
10 cy ATTN: C. Rino

Teledyne Brown Engineering
ATTN: R. Deliberis

Tri-Com, Inc.
ATTN: D. Murray

TRW Defense & Space Sys. Group
ATTN: S. Altschuler
ATTN: R. Plebuch
ATTN: D. Dee

Utah State University
ATTN: L. Jensen
ATTN: K. Baker

Visidyne, Inc.
ATTN: J. Carpenter

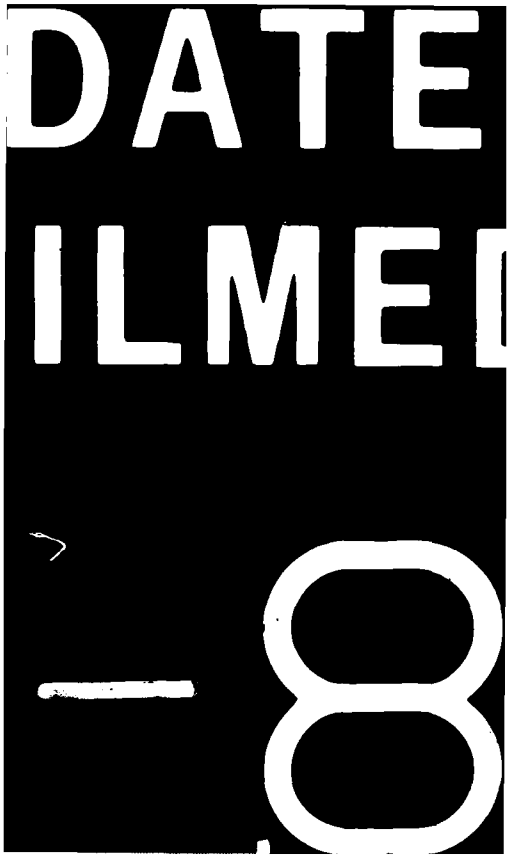
DATE
ILME
8